Journal of Power Sources 245 (2014) 1–6

Contents lists available at SciVerse ScienceDirect

Journal of Power Sources

journal homepage: www.elsevier.com/locate/jpowsour

# A method of separating the capacities of layer and spinel compounds in blended cathode

Takeshi Kobayashi*, Norihiro Kawasaki, Yo Kobayashi, Kumi Shono, Yuichi Mita, Hajime Miyashiro

*Materials Science Research Laboratory, Central Research Institute of Electric Power Industry, 2-11-1 Iwado-kita, Komae, Tokyo 201-8511, Japan*

## HIGHLIGHTS

- Blended cathodes are fabricated from a layer compound and a spinel compound.
- Capacity curve of a blended cathode is differentiated by the voltage (d*Q*/d*V*).
- Blended cathode is expressed using d*Q*/d*V* curves of the two active materials.
- Layer compound d*Q*/d*V* curve is calculated using the curve in the blended cathode.
- This method leads to capacity separation of active materials from blended cathode.

## GRAPHICAL ABSTRACT

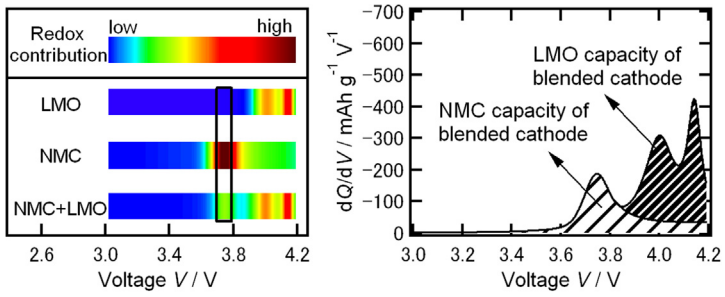


## ARTICLE INFO

*Article history:*
Received 8 April 2013
Received in revised form
6 June 2013
Accepted 7 June 2013
Available online 27 June 2013

*Keywords:*
Lithium-ion battery
Blended cathode
Layer compound
Spinel compound
Differential analysis
Degradation analysis

## ABSTRACT

Some mixtures of two active materials are utilized for the blended cathodes in lithium-ion batteries. The blended cathode and unitary cathodes were prepared by a layer compound, $LiNi_{1/3}Mn_{1/3}Co_{1/3}O_2$, and a spinel compound, $LiAl_{0.1}Mn_{1.9}O_4$ as simple active materials in order to develop the method to estimate the capacities of the both active materials in the blended cathode. The differential curves (d*Q*/d*V*) clearly provided the information on the redox voltage region of the layer and the spinel compounds in the unitary and blended cathodes. A regression curve of the layer compound was partially calculated using the d*Q*/d*V* of blended cathode in the layered redox voltage region, and it was extrapolated until the mixed redox voltage region of the layer and spinel compounds. The capacity in the blended cathode was divided into the capacities of the active materials by this curve. This method was also successfully applied to the degraded blended cathode. This method proposed in this paper is a significant technique for degradation analysis of both active materials in the blended cathode without the need for the same active material lots as those of blended cathodes, using information on electrochemically active voltage ranges of each active material such as references.



## 1. Introduction

Lithium-ion batteries have been used as rechargeable energy sources in many devices such as mobile phones, laptop computers, and hybrid electric vehicles. High power density, high energy density, excellent charge–discharge cycling performance, and sufficient safety are necessary for the lithium-ion battery because of the increase in the demands of highly functionalized applications. One of the key materials in characterizing the battery design is the cathode material. For example, layer compounds [1–3] have been selected for high-energy uses, spinel compounds [4] have been

* Corresponding author. Tel.: +81 3 3480 2111; fax: +81 3 3480 3401.
*E-mail address:* kobatake@criepi.denken.or.jp (T. Kobayashi).

0378-7753/$ – see front matter © 2013 Elsevier B.V. All rights reserved.
http://dx.doi.org/10.1016/j.jpowsour.2013.06.039

selected in cases of low cost and/or high power, and olivine compounds [5] have been selected for high power and long-life requirements. These compounds have advantages and disadvantages in terms of their properties, such as capacity, power, toxicity, safety, and cost. However, there is no cathode material that satisfies all of the above properties simultaneously. Some researchers have reported the blending of two cathode materials to compensate for the mutual disadvantage of two active materials such as low energy, high cost by their advantage in the blended cathode [6,7]. The suppression of $Mn^{2+}$ dissolution from $LiMn_2O_4$ spinel compound by blending $LiNi_{0.8}Co_{0.2}O_2$ into the spinel compound has been reported in attempts to improve charge–discharge cycling performance. Numata et al. confirmed the decrease in $Mn^{2+}$ concentration in the electrolyte after the storage at high temperature as a result of the active material blending [7]. However, the degradation analysis of lithium-ion batteries with blended cathodes is more complicated when trying to elucidate the degradation mechanism compared with the case of unitary cathodes. The degradation analysis of the cathode in lithium-ion batteries has been carried out by X-ray photoelectron spectroscopy, XPS [8], Transmission electron microscopy, TEM [9], Scanning electron microscopy, SEM coupled with Energy dispersive X-ray analysis, EDX [10], Electron energy-loss spectroscopy, EELS [11], X-ray absorption fine structure, XAFS [12], and ac impedance spectroscopy [13]. The change in the chemical form of the transition metal ions, such as nickel, cobalt, and manganese, residual product deposited on the cathode, structural collapse on the particle surface, dissolution of the transition metal ion, and increase in the impedance of lithium-ion diffusion in the interfacial/internal cathode have been investigated by the above techniques. We can qualitatively explain the degradation mechanism of the cathodes using the above multilateral approach. However, the correlation between the qualitative degradation mechanism and its quantitative capacity degradation ratio in the battery is not discussed completely. The remaining capacity in the lithium-ion battery is more important for users to operate the application devices and to predict the battery life rather than the degradation factors. Separating the capacities of the two active materials in the degraded blended cathode is also important to estimate quantitatively the cathode degradation analysis in detail. The use of the discharge voltage curve versus capacity in the blended cathode of the half-cell is simple and practicable for the evaluation of the capacities of the two active materials. However, it is not easy to estimate the capacities from the blended cathode discharge curve when the redox potentials of the two active materials overlap in the discharge voltage range. Thus, it would be effective to apply a differential analysis to the above overlapped blended cathode discharge data in order to understand the discharge characteristics for the two active materials in the blended cathode and to determine the differences between the two active materials. This is because the use of the differential is an effective method of emphasizing delicate changes. The differential analysis has been reported to be applied to lithium-ion batteries [14,15]. This method leads to an improvement in the prediction of the lifetime of the lithium-ion battery compared with the commonly used root rule [14]. Bloom et al. researched the degradation content of both the cathode and the anode in lithium-ion batteries by the differential method [15]. However, there is no report on applying the differential method to estimate the capacities of the two active materials in a blended cathode. Therefore, in this study, layer and spinel unitary cathodes, and a mixed cathode were prepared to obtain the discharge voltage versus capacity curves. Cathode materials were selected to develop the method to estimate their capacities in the blended cathode because the estimation of their capacities is very challenging approach from the differential curve in the blended cathode. $LiNi_{1/3}Mn_{1/3}Co_{1/3}O_2$ (NMC) was selected as a model cathode for the layer compound because it has a very simple discharge curve on which to apply the differential method. Al-substituted $LiAl_{0.1}Mn_{1.9}O_4$ (LMO) was selected for the spinel compound because $Mn^{2+}$ dissolution is suppressed. We tried to develop a method of separating the capacity of the nondegraded/degraded blended cathode into the capacities of the unitary cathodes on the basis of information on the differential curves and electrochemically active voltage ranges of each active material cathodes.

## 2. Experimental

NMC and LMO were prepared for the layer compound and the spinel compound of unitary active material (AM) cathodes. A blended cathode active material was fabricated by mixing the two AMs in the weight ratio of NMC:LMO = 30:70 using an agate mortar. An electrode with the blended cathode active material was abbreviated as NML37. Slurries were fabricated with the cathode active materials, acetylene black (AB), vapor grown carbon fiber (VGCF), and polyvinylidene fluoride (PVdF) dissolved in N-methylpyrrolidone (NMP) in the weight ratio of AM:AB:VGCF:PVdF = 85:3:3:9 wt%. The slurries were applied on an aluminum collector, and dried to remove the NMP at 100 °C. Subsequently, the electrodes of $\varphi$ 16 mm were cut out. The AM weight was ca. 2 mg per square centimeter. The thickness of the electrodes was ca. 10 μm. The electrodes were dried under vacuum at 85 °C overnight and then stored under argon atmosphere. 2032 coin-type cells were fabricated with the above cathodes as working electrodes, 1 M lithium hexafluorophosphate ($LiPF_6$) in ethylene carbonate (EC)/dimethyl carbonate (DMC) as the liquid electrolyte, lithium metal as the counter electrode, and a polyethylene separator under argon atmosphere. These cells were tested between 3.0 and 4.2 V at C/20 to minimize capacity decrease due to cell polarization, with the rest time (or relaxation time) between charge and discharge being 10 min. The estimated nominal capacities of NMC and LMO were defined as 150 and 100 mAh $g^{-1}$, respectively, to specify the applied current at C/20. The nominal capacity of NML37 was estimated to be 115 mAh $g^{-1}$ using the capacities and the weight ratios of the NMC and the LMO. These cells were charge–discharged at 1C for 300 cycles at 50 °C to obtain the degraded data at short times, then tested at C/20 at 25 °C for 3 cycles. A biologic VMP3 was used for the charge–discharge tests. The data of the 3rd cycle at C/20 were used to analyze the capacity from voltage curves.

The morphology of the particles was investigated by a scanning electron microscopy (SEM; FEI QUANTA 250). The elemental composition of Al/Ni/Mn/Co/O in the cathode was determined by EDX (EDAX GENESIS2). The element compositions were determined from the integral of the Kα peaks. The active materials in the cathode were characterized by powder X-ray diffraction (XRD; Rigaku TTR-III) measurements using 15 kW Cu$K_\alpha$ radiation. The compounds in the cathode were quantitatively estimated by Rietveld refinement (Rietan-FP) [16].

## 3. Results and discussion

### 3.1. Proposal for capacity separation in the blended cathode

The cathode materials, including the active materials and conductive materials, were separated from the aluminum collector using carbon tape. Fig. 1 shows the SEM image of NML37, the EDX mapping of the particles, and the EDX spectra for particles A and B in NML37. Different particle morphologies were found on the cathode in Fig. 1 (×5000). In the same observed area, different elements were distributed in the two kinds of particles, as revealed by the combination of SEM observation and EDX area mapping. The elements were identified from kα spectra of EDX analysis. Some

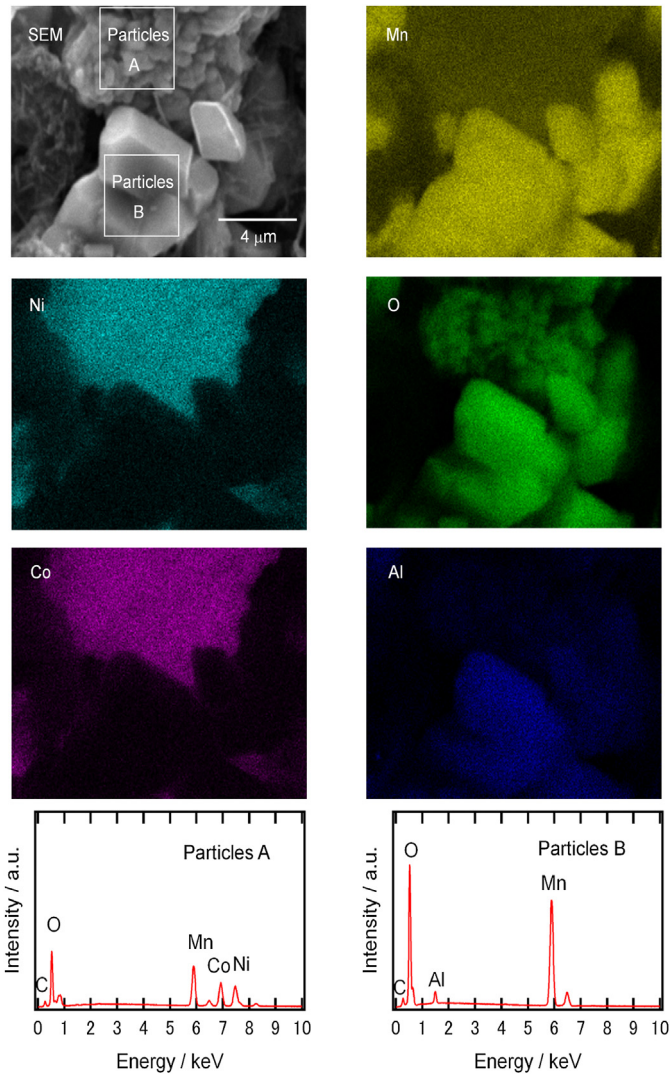


**Fig. 1.** SEM image and corresponding energy dispersive X-ray spectroscopy (EDX) mappings of cobalt, manganese, nickel, aluminum, and oxygen in the blended cathode, NML37, and EDX spectra of particles A and particles B.

unlabeled peaks originated from the kβ or Lα spectra. Particle A was composed of nickel, manganese, cobalt, and oxygen, as determined from the EDX spectrum. On the other hand, particle B was composed of aluminum, manganese, and oxygen. The aluminum to manganese element molar ratio was Al:Mn = 1:19 from the EDX analysis result of a very small range of particle B (×40,000) while the element molar ratio, Ni:Mn:Co was 1:1:1 in particle A (×40,000). Particle A was identified as $LiNi_{1/3}Mn_{1/3}Co_{1/3}O_2$ (NMC), and particle B was $LiAl_{0.1}Mn_{1.9}O_4$ (LMO).

The X-ray diffraction pattern was obtained for the cathode to identify the compounds. Fig. 2 shows the observed, calculated and difference diffraction patterns of the cathode material obtained by Rietveld refinement. The refinement result indicated that the mass fraction ratio of two compounds was NMC:LMO = 31:69. This value obtained by Rietveld refinement, was coincident with that of the prescribed weight ratio (NMC:LMO = 30:70). The active materials and weight ratios in the blended cathode with NMC and LMO compounds were ascertained by the combination of SEM observation, EDX analysis, and XRD/Rietveld refinement. These analyses are expected to be significant technique to obtain the unknown cathode information in the commercial lithium-ion battery. The

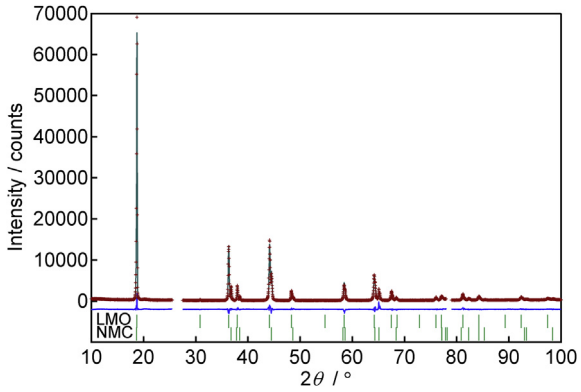


**Fig. 2.** Observed (symbols), calculated (solid line), and difference (bottom) profiles for the Rietveld refinement of X-ray diffraction data of the layer compound and the spinel compound in the blended cathode. The short vertical lines below profiles indicate the peak positions of all possible Bragg reflections. $R_{wp}$ = 7.9%, $S$ = 1.9, $R_B$(LMO) = 1.7%, $R_B$(NMC) = 1.9%.

cathode information included NMC and LMO obtained from these analyses facilitates identifying the some peaks of the differential curves in the blended cathode, NML37.

To separate the capacities of the blended cathodes into the capacities of the two compounds, the cells were charge–discharged using the NMC, the LMO, and the NML37. Fig. 3 shows the discharge voltage curves versus the capacity, the curves of differential capacities with respect to cell voltages (d$Q$/d$V$) of the NMC, the LMO, and the NML37, and the dependence of the redox contribution on the voltage in the cells with NMC and LMO. The differential curves of NMC and LMO were also normalized by the weight ratios of NML37. The obtained capacities of NMC, LMO, and NML37 were 156, 92, and 110 mAh $g^{-1}$, respectively. The capacities of the blended cathode were found to be calculable from the sum of the weight ratios and the capacities of the unitary AMs (156 mAh $g^{-1}$ × 0.3 + 92 mAh $g^{-1}$ × 0.7 = 111 mAh $g^{-1}$). The voltages of the differential peaks for both unitary AMs were almost coincident with those of NML37 in Fig. 3(b). This indicated that the redox potentials of unitary AMs exhibited no significant effect upon blending. The differential curves of the NMC and the LMO are drawn in Fig. 3(b) normalized by the weight ratios of the AMs in NML37. The normalized differential curve of NMC was partially coincident with that of NML37 under 3.85 V in the voltage region.

The separation of the capacities of the blended cathode into the capacities of two unitary AMs was attempted using the d$Q$/d$V$ curve of the blended cathode on the basis of the electrochemical characteristics for the two AMs. Here, the concept of the method is described using the characteristics of the electrochemical reactions for LMO and NMC in Fig. 3(c). Red in the color bar of the cathode corresponds to a high redox contribution of the cathode. The color bar was derived using the d$Q$/d$V$ values of NMC and LMO. This redox contribution of the cathode corresponds to the current in the cyclic voltammogram. LMO has two peaks at voltage peak positions of 4.0 V and 4.14 V. On the other hand, NMC has only one peak at 3.75 V that decreases monotonically during the charging process. The electrochemical reaction of NMC occurs in a wide voltage range between 3.5 and 4.2 V, whereas that of LMO occurs in a limited voltage range between 3.85 and 4.2 V. Some researchers have estimated these electrochemical behaviors for the NMC and the LMO [17,18] using the cyclic voltammogram. The CV peaks of LMO were 4.0 and 4.1 V while that of NMC was 3.64 V. The difference in these values of NMC between this paper and the reference may originate from the scan rate of the CV and the C-rate during the discharging process. Fundamentally, the d$Q$/d$V$ curves and

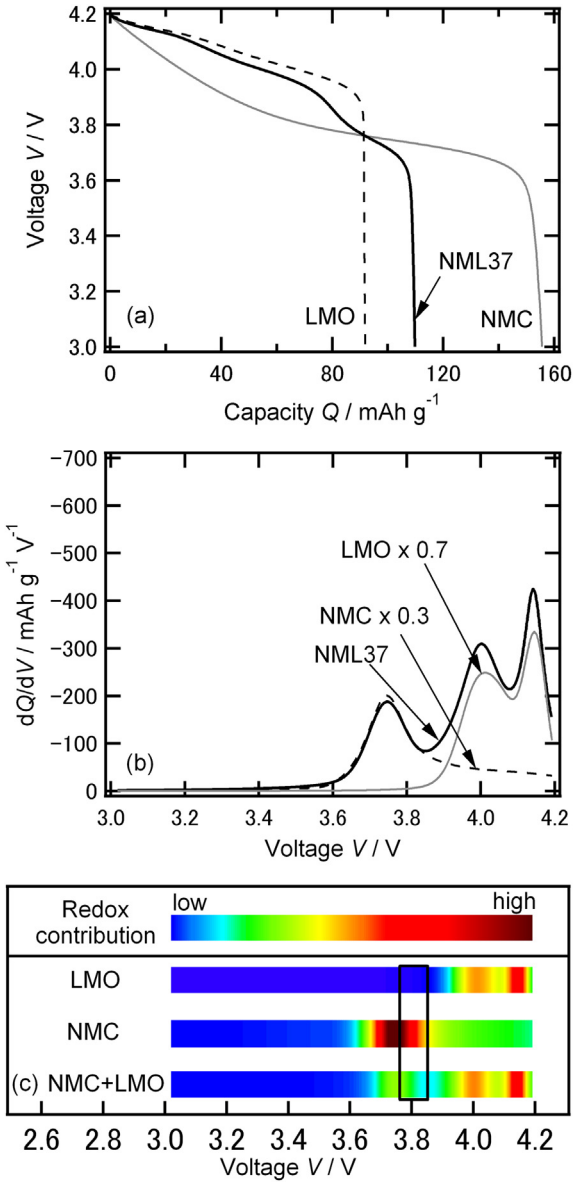


**Fig. 3.** (a) Discharge curves, (b) differential capacity curves (d$Q$/d$V$) versus voltage for NMC, LMO, and NML37 cells measured at 25 °C under a C/20 rate, and (c) concept of separating the blended cathode capacity. The colors correspond to the redox contributions of NMC, LMO, and NML37 depending on the voltage in the cells. The greater the amount of red in the color bar of the cathode, the higher the redox contribution of the cathode. The rectangle outlines the important voltage region between 3.75 and 3.85 V for the concept. (For interpretation of the references to color in this figure legend, the reader is referred to the web version of this article.)

electrochemically active voltage ranges of the other NMC and LMO shown in the quote from the references [17,18] should be almost same as those of NMC and LMO in this study. Thus, it is possible to determine the electrochemically active voltage range of NMC only in the blended cathodes, NML37 not using raw data of the same unitary active materials cathodes as those of blended cathodes, but, of course, using information on the d$Q$/d$V$ shape and the electrochemically active voltage range of NMC and LMO such as the references. We compared each d$Q$/d$V$ peak of NMC and LMO and concluded that the voltage range below 3.85 V in the blended cathode could be attributed to the reaction of only NMC. In other words, NMC and LMO reactions were overlapped at higher voltage than 3.85 V. Then, we tried to extract the contribution of LMO at higher voltage than 3.85 V by extrapolating the d$Q$/d$V$ decay of NMC. Therefore, it is necessary to find the electrochemically active voltage range of NMC in order to calculate the d$Q$/d$V$ curve of only NMC in the blended cathode at higher voltage than 3.85 V. The applied voltage range for the extrapolation was determined from the intersection point of the quadratic differential curve ($d^2Q/dV^2$ *vs* $V$) of NML37 and the zero axis of $d^2Q/dV^2$, as shown in Fig. 4(a). Zero points of the quadratic differential curve of NML37 mean the maximum/minimum points and the folding point of first differential curve corresponding to the change in the electrochemical reactions. The selected range discharging by NMC only was between 3.75 and 3.85 V. This range was determined from the quadratic differential curve on the basis of the electrochemical characteristics of NMC and LMO. These characteristics were also possible to obtained from the reference such as [17,18] not using the raw data of the NMC and LMO. Then, the d$Q$/d$V$ curve of NMC in NML37 was

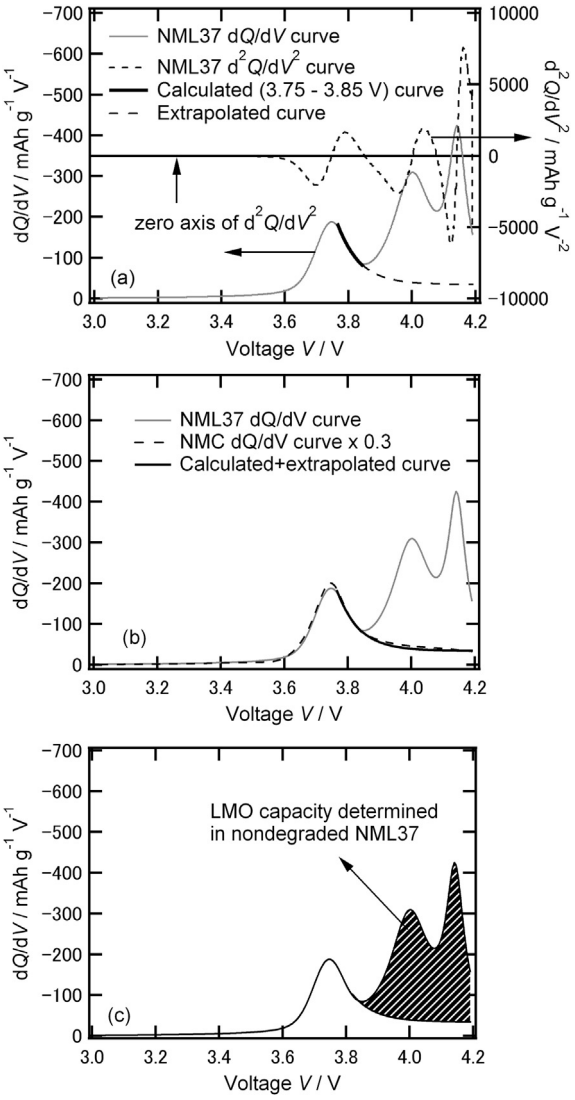


**Fig. 4.** (a) Differential curve (d$Q$/d$V$) and quadratic differential curve ($d^2Q/dV^2$) for NML37, the curve calculated using the d$Q$/d$V$ data between 3.75 V and 3.85 V, and d$Q$/d$V$ curve extrapolated to discharge start voltage, (b) d$Q$/d$V$ curves for NML37, and NMC × 0.3, and combination of the calculated and extrapolated curves. (c) d$Q$/d$V$ curve of NML37 including the LMO capacity in NML37 determined by the separation of the d$Q$/d$V$ curve using the extrapolated curve. The capacities determined by this method were 66 mAh $g^{-1}$ (LMO) and 44 mAh $g^{-1}$ (NMC). Those calculated using the weight ratios and the unitary data were 65 mAh $g^{-1}$ (LMO) and 47 mAh $g^{-1}$ (NMC).

extrapolated from 3.85 V to 4.2 V using the d$Q$/d$V$ curve of NMC in NML37 in the voltage range between 3.75 and 3.85 V. Thus, the parameters of the recurrent curve were calculated to express the d$Q$/d$V$ curve of NMC using the d$Q$/d$V$ data of NML37 between 3.75 V and 3.85 V. An exponential function was selected for the simple recurrent curve model to express the d$Q$/d$V$ monotonic decrease of NMC, which was found to include in the cathode by above analyses in advance [19], and the measured NMC decay curve was well reproduced by extrapolation of the calculated exponential curve as shown in Fig. 4(b). Finally, the d$Q$/d$V$ curve of unitary NMC between 3.85 and 4.2 V was reconfirmed by the extrapolation of the partial d$Q$/d$V$ curve of NML37 in Fig. 4(c), and successfully reproduced the capacity separation curve between NMC and LMO. This means that the first/quadratic differential and the extrapolating method are effective in separating the blended cathode capacity into the capacities of the two AMs. The capacities of LMO and NMC in NML37 were calculated to be 66 mAh $g^{-1}$ and 44 mAh $g^{-1}$, respectively, applying our method to the NML37 discharge curve (capacity *vs* voltage). These values were almost coincident with 65 mAh $g^{-1}$ (LMO) and 47 mAh $g^{-1}$ (NMC) calculated using the capacities and weight ratios of LMO and the NMC. The error in the maximum relative capacity calculated by this method was within 6% against the measured data for LMO and NMC.

### 3.2. Application of our method to the degraded blended cathode

This method was applied not only to the nondegraded data, but also to the degraded data of the blended cathode. Fig. 5 shows the discharge curves (capacity *vs* voltage) of the nondegraded and degraded cathodes, and the differential curve (d$Q$/d$V$) of NML37. The cells were degraded by accelerating the capacity decrease at 50 °C for 300 cycles. The capacities at C/20 of the degraded NMC, LMO, and NML37 were 135, 86, and 99 mAh $g^{-1}$, respectively. The capacity calculated using the capacities and the weight ratios of the degraded NMC and LMO (135 mAh $g^{-1}$ × 0.3 + 86 mAh $g^{-1}$ × 0.7 = 101 mAh $g^{-1}$) was similar to the measured capacity of NML37 (99 mAh $g^{-1}$). Our method using the above-proposed procedure was applied to the differential data (d$Q$/d$V$) to separate the capacities of the degraded NMC and LMO. The capacity of the degraded LMO determined by this method was 57 mAh $g^{-1}$, which is similar to the capacity calculated of 60 mAh $g^{-1}$ using the decreased capacity value and the weight ratio of the degraded LMO. In addition to NML37, this method was successfully applied to the determination of the capacity ratio of the NMC and the LMO in other blended cathodes with good accuracy (Fig. 6) [19]. Some researchers have reported the suppression of the capacity decrease of the spinel by blending it with the $LiNi_{0.8}Co_{0.2}O_2$ compound [6,7]. However, we obtained no positive effect of suppressing the capacity decrease of LMO in this study. The reason for the difference between the results of this study and the previous studies may be that (i) aluminum was partially substituted into the spinel compound to suppress the dissolution of manganese ions from the compound or (ii) the degradation test conditions were inadequate for confirming the blending effect. This method was found to be able to separate the capacities of LMO and NMC of the nondegraded and degraded blended cathodes, on basis of information of electrochemically active voltage range of NMC and LMO without the need to prepare the unitary same AM lots as those of the blended cathode, with information on electrochemically active voltage ranges of NMC and LMO. The applied blended cathode is limited to be NMC/LMO system by this method, although the method seems to be possible to be applied into other blended cathode with a AM of monotonic decrease curve such as NMC in the voltage range which both AMs are electrochemically active. Currently, we are technically trying whether this method are applied into the blended cathode of the

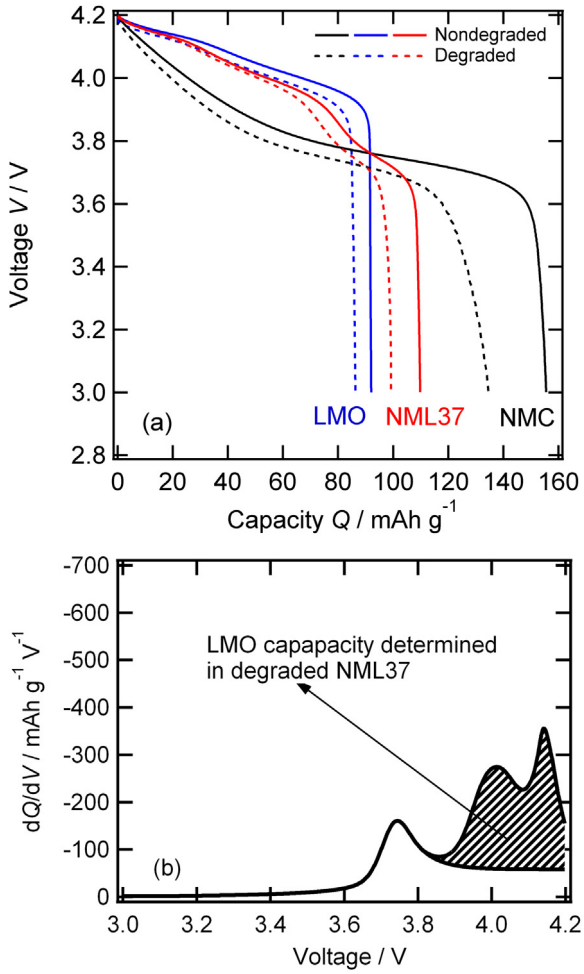


**Fig. 5.** (a) Discharge curves at C/20 for NMC, LMO, and NML37 before and after 300 cycles at 1C. The solid curves and the dashed curves show the discharge curves in the cells using the nondegraded and degraded cathodes for NMC (black), LMO (blue), and NML37 (red). (b) d$Q$/d$V$ curve of degraded NML37 including the LMO capacity in degraded NML37 determined by separation of the d$Q$/d$V$ curve using the extrapolated curve. (For interpretation of the references to color in this figure legend, the reader is referred to the web version of this article.)

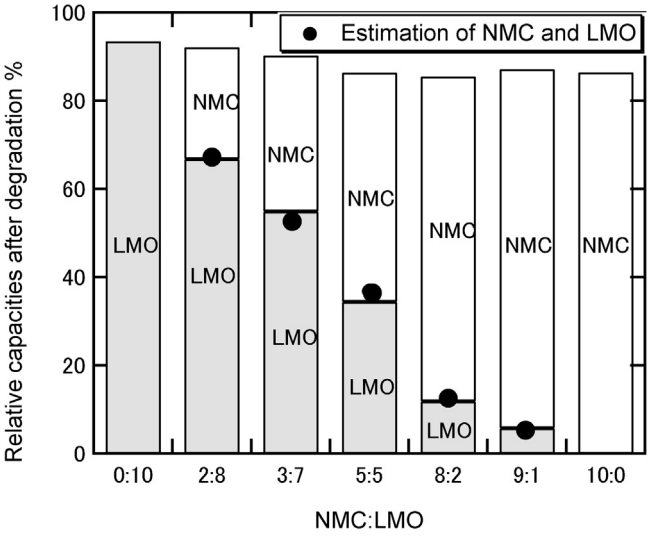


**Fig. 6.** Relative capacities of degraded cell, NMC, and LMO in various blended cathodes calculated by capacities and weight ratios of two active materials. Circles show the estimation of capacity boundaries between NMC and LMO.

other materials with a AM of non-monotonic decrease d$Q$/d$V$ curve in the voltage range.

## 4. Conclusion

The capacity ratio of each of two active materials in a blended cathode was determined by comparing the capacities of a layer compound, $LiNi_{1/3}Mn_{1/3}Co_{1/3}O_2$ (NMC), spinel compound, $LiAl_{0.1}Mn_{1.9}O_4$ (LMO), and their blended cathode. The differential curve in the selected voltage range, which was confirmed only the redox reaction of NMC, was extrapolated to the discharge start voltage, and the capacity of LMO could be obtained. This extrapolating approach using a differential curve of the voltage enables the determination of separating NMC and LMO capacities. The LMO capacity in the blended cathode estimated by this method showed good agreement with the value calculated from the weight ratio and the capacity of the cell with only LMO. The capacity estimation of two active materials was effective for not only the nondegraded, but also the degraded blended cathode by this method without the discharge data of the cells using two active materials. The method paved the way for the quantitative estimation of unitary active materials in the blended cathode of lithium-ion batteries.

## Acknowledgment

The authors appreciate Mr. Yasutaka Ohno of Electric Power Engineering Systems Co., Ltd. for his technical support.

## References

[1] K. Mizushima, P.C. Jones, P.J. Wiseman, J.B. Goodenough, Mater. Res. Bull. 15 (1980) 783–789.
[2] J.P. Peres, F. Weill, C. Delmas, Solid State Ion. 116 (1999) 19–27.
[3] T. Ohzuku, Y. Makimura, Chem. Lett. 30 (2001) 642–643.
[4] J.M. Tarascon, W.R. Mckinnon, F. Coowar, T.N. Bowmer, G. Amatucci, D. Guyomard, J. Electrochem. Soc. 141 (1994) 1421–1431.
[5] A.K. Padhi, K.S. Nanjundaswamy, J.B. Goodenough, J. Electrochem. Soc. 144 (1997) 1188–1194.
[6] N. Imachi, K. Saishou, S. Nakamizo, H. Watanabe, S. Narukawa, The 40th Battery Symposium in Japan, 2C12 (1999), pp. 297–298.
[7] T. Numata, C. Amemiya, T. Kumeuchi, M. Shirakata, M. Yonezawa, J. Power Sources 97–98 (2001) 358–360.
[8] D. Aurbach, B. Markovsky, A. Rodkin, E. Levi, Y.S. Cohen, H.J. Kim, M. Schmidt, Electrochim. Acta 47 (2002) 4291–4306.
[9] H. Gabrisch, T. Yi, R. Yazami, Electrochem. Solid-State Lett. 11 (2008) A119–A124.
[10] H. Zheng, Q. Sun, G. Liu, X. Song, V. Battaglia, J. Power Sources 207 (2012) 134–140.
[11] S. Muto, K. Tatsumi, Y. Kojima, H. Oka, H. Kondo, K. Horibuchi, Y. Ukyo, J. Power Sources 205 (2012) 449–455.
[12] H. Kobayashi, M. Shikano, S. Koike, H. Sakaebe, K. Tatsumi, J. Power Sources 174 (2007) 380–386.
[13] M. Kassem, J. Bernard, R. Revel, S. Pelissier, F. Duclaud, C. Celacourt, J. Power Sources 208 (2012) 296–305.
[14] K. Honkura, K. Takahashi, T. Horiba, J. Power Sources 196 (2011) 10141–10147.
[15] I. Bloom, A.N. Jansen, D.P. Abraham, J. Knuth, S.A. Jones, V.S. Battaglia, G.L. Henriksen, J. Power Sources 139 (2005) 295–303.
[16] F. Izumi, K. Momma, Solid State Phenom. 130 (2007) 15–20.
[17] Y. Shao-Horn, R.L. Middaugh, Solid State Ion. 139 (2001) 13–25.
[18] M. Wang, Y. Chen, F. Wu, Y. Su, L. Chen, D. Wang, Electrochim. Acta 55 (2010) 8815–8820.
[19] T. Kobayashi, K. Shono, Y. Kobayashi, H. Miyashiro, Y. Mita, CRIEPI Report, Q11022 (2012) (in Japanese).